

## Water Resources Research

### RESEARCH ARTICLE

10.1002/2017WR020385

#### Key Points:

- Novel method for stochastic design of groundwater monitoring network
- Null-space Monte Carlo simulation combined with reduced-rank spatial prediction and Differential Evolution for optimizing well locations
- Reduced-rank spatial prediction helps to drastically reduce the computational burden of the monitoring network design problem

#### Correspondence to:

J. Sreekanth,  
sreekanth.janardhanan@csiro.au

#### Citation:

Sreekanth, J., H. Lau, and D. E. Pagendam (2017), Design of optimal groundwater monitoring well network using stochastic modeling and reduced-rank spatial prediction, *Water Resour. Res.*, 53, 6821–6840, doi:10.1002/2017WR020385.

Received 11 JAN 2017

Accepted 17 JUL 2017

Accepted article online 20 JUL 2017

Published online 12 AUG 2017

## Design of optimal groundwater monitoring well network using stochastic modeling and reduced-rank spatial prediction

J. Sreekanth<sup>1</sup> , Henry Lau<sup>2</sup>, and D. E. Pagendam<sup>2</sup>

<sup>1</sup>CSIRO Land and Water, Dutton Park, Queensland, Australia, <sup>2</sup>CSIRO Data 61, Dutton Park, Queensland, Australia

**Abstract** A method for the stochastic design of groundwater quality observation well network is presented. The method uses calibration-constrained Null-space Monte Carlo analysis for the stochastic simulation of the reduction ratio of peak concentration and the time corresponding to this in an injection well field. The numerical groundwater model simulations are constrained with a limited amount of field measurements. The objective of the monitoring network design is to identify optimal monitoring locations that allow for prediction of spatial fields from the data collected at limited number of points in the spatial domain. These locations need to be robust to different possible outcomes simulated using the stochastic model runs, and result in good spatial predictions, regardless of which one of the many possibilities turned out to be the true representation of nature. Multiple simulated fields of concentration and time are used to identify a small set of empirical orthogonal functions (spatial basis functions) for reduced-rank prediction of the spatial patterns in these two fields. The Differential Evolution algorithm was used to find the monitoring locations that allowed for optimal reconstruction of all the simulated fields (potential future states of reality) from the set of empirical orthogonal functions. The applicability is demonstrated for designing a monitoring network for an injection well field. Optimal locations of 10 monitoring wells were identified. The method has the capability to simultaneously identify the optimal locations and inform optimal times for monitoring reduction ratio of peak concentration. The method is flexible to iteratively combine stochastic modeling and monitoring for optimal groundwater management.

**Plain Language Summary** Groundwater data collection from monitoring wells is important for evaluation of impacts from resource development. When and where to place a monitoring well to collect these data is an important decision to make for groundwater managers, primarily because groundwater monitoring is expensive. Mathematical modeling can provide predictive information about potential water quality changes arising from resource development. However, often there is large uncertainty in these predictions which makes it difficult to make the basis for investment decisions. In this study, we propose a novel method for optimizing monitoring network design in which many plausible future outcomes of water quality are considered and synthesized to help the design of monitoring network.

### 1. Introduction

Coal seam gas (CSG; coal bed methane) is widely recognized as a potential unconventional energy resource in many parts of the world. CSG development on an accelerated commercial scale has recently commenced in Australia [Flemming and Measham, 2015]. CSG production from several sedimentary basins of Australia will result in the extraction of large volumes of water [Nghiem et al., 2011]. Reinjection of the CSG produced water into aquifers of good water quality, after necessary treatment, is an option that would allow its use by both industry and regulatory agencies, however, a major risk of these managed recharge schemes is the potential for water quality changes caused by accidental contamination or hydrochemical changes caused by the injected water. Such large-scale reinjection schemes often involve injection well fields consisting of many wells spread over a large geographic area. The Australian Government has identified reinjection of coproduced water into aquifers as potential hazard *National Water Quality Management Strategy* [2014]. Regulatory requirements, as per *National Water Quality Management Strategy* [2014], stipulate that continuous monitoring is implemented for detection and management of potential water quality change. Groundwater flow and transport models are widely used to simulate the potential water quality impacts of

proposed resource development activities. The information provided by such models may be used for the design of targeted monitoring networks for monitoring. A novel method that integrates stochastic simulation using numerical groundwater flow and transport models (MODFLOW and MT3DMS) and reduced-rank spatial prediction for optimizing monitoring network design is proposed in this study.

A major challenge in the application of numerical models for management decisions is the inherent uncertainty in predictions caused by model structural and parameter uncertainty, and from the inadequate characterization of the subsurface system [Sreekanth and Datta, 2011; Sreekanth et al., 2012]. Hence, investigation of the impacts of a development activity using dedicated water quality monitoring networks is important for the detection of any undesirable change as well as for minimization of the uncertainty and better characterization of the system.

Past studies have considered different groundwater quality monitoring objectives. These include minimizing the variance of a statistical estimator [McKinney and Loucks, 1992; Asefa et al., 2004, 2005; Nunes et al., 2004a, 2004b; Herrera and Pinder, 2005; Ammar et al., 2008; Chadalavada and Datta, 2008; Dokou and Pinder, 2009; Ruiz-Cárdenas et al., 2010; Chadalavada et al., 2011], contaminant detection [Massmann and Freeze, 1987a, 1987b; Meyer and Brill, 1988; Hudak and Loaiciga, 1992, 1993; Datta and Dhiman, 1996; Mahar and Datta, 1997; Storck et al., 1997; Montas et al., 2000; Reed et al., 2000, 2003; Nunes et al., 2004a, 2004b; Reed and Minsker, 2004; Wu et al., 2006; Kollat and Reed, 2007; Kollat et al., 2008, 2011], and minimization of mass estimation error [Montas et al., 2000; Reed and Minsker, 2004; Wu, 2004; Wu et al., 2006; Kollat and Reed, 2007]. A careful observation of these objectives reveals that the two major factors that necessitate the design of an optimal monitoring network are (i) minimizing uncertainty in the prediction of the contaminant plume and (ii) minimizing the costs involved in conducting the monitoring. Thus, maximizing the value of the data collected or "data-worth" while satisfying the budgetary constraints has been one of the primary purposes of most monitoring schemes. Cost is often one of the largest constraints preventing extensive groundwater quality monitoring. A number of studies have also looked at the cost-effective design of monitoring networks [Loaiciga et al., 1992; James and Gorelick, 1994; Sreekanth and Datta, 2013; Alzraiee et al., 2013].

A key consideration for maximizing the data-worth is elimination of redundancy in the data collected. Many past monitoring network designs focused on the spatial data collection by optimizing the monitoring well locations [Reed et al., 2000; Reed and Minsker, 2004; Bierkens, 2006; Dhar and Datta, 2009]. More comprehensive designs, consider minimization of spatiotemporal redundancy in the monitoring data. Cameron and Hunter [2000] proposed an approach that used two separate algorithms for reducing spatial and temporal redundancies. The space-time cross correlation of contaminant concentration was not considered in that study.

Herrera and Pinder [1998] proposed a method that used the Kalman filter together with stochastic simulation of contaminant transport for spatiotemporal optimization of monitoring networks. The Kalman filter was used to calculate the reduction in the variance of predicted concentrations when a sample was taken from a monitoring well at a particular time. This method was found to be promising and has since been applied in a number of later studies including Herrera et al. [2000], Herrera and Pinder [2005], Zhang et al. [2005], and Dokou and Pinder [2009]. Alzraiee et al. [2013] extended the design method for multiobjective aquifer monitoring networks, where both spatial prediction of the groundwater head field and geostatistical parameter estimation are the foci. These studies considered a space-time vector of contaminant concentrations and a resulting space-time covariance matrix. The covariance matrix is updated using the "Kalman gain" from a new sampling location/time and the concentration distribution is reestimated. When applied to long-term monitoring network designs for field scale applications this approach may have to deal with very large space-time covariance matrices. Often, potential monitoring locations are preselected to reduce the dimensionality of the problem [Herrera and Pinder, 2005; Herrera and Simuta-Champo, 2013].

### 1.1. Overview of the Research Approach

The main objective of this study is the development of a novel method for the design of purpose-built groundwater well networks for monitoring water quality compliance. The objective of the monitoring network design is to identify optimal monitoring locations that allow for prediction of spatial fields from the data collected at limited number of points in the spatial domain. These locations need to be robust to different possible outcomes simulated using the stochastic model runs, and result in good spatial predictions, regardless of which one of the many possibilities turned out to be the true representation of nature. The

method uses calibration-constrained stochastic simulations of the groundwater flow and transport. The predictive simulations are then used to identify sampling locations that provide maximum data-worth for ensuring water quality compliance and helps minimize uncertainty surrounding two model predictions. These are prediction of (1) the ratio of peak concentration realized at any location in the well field within a specified simulation period to the injected concentration and (2) the time corresponding to the peak concentration ratio. These variables are respectively referred to as peak concentration and peak time in the remainder of this paper. The proposed method helps to identify optimal locations at which observations will provide robust predictions of peak concentration and time of peak concentration arrival across the entire spatial domain. Peak concentration is considered important from a regulatory perspective for the assessment of environmental and public health risks [Bolster *et al.*, 2009]. It is also important for studying the attenuation characteristics of the contaminant plume. The proposed method relies on the initial characterization of the contaminant plume using stochastic groundwater flow and transport modeling. The novelties of the proposed method are as follows. First, the spatiotemporal monitoring network design uses predictions from calibration-constrained stochastic simulation of the contaminant plume movement. Thus, the design considers all available prior information on the groundwater flow and transport system. Second, the proposed method targets the detection of peak concentration and peak arrival time at any location while also accounting for uncertainties in the groundwater system dynamics. This has potential applicability in terms of environmental and public health risk assessment. Finally, the method does not assume that the monitoring wells should be selected from a predetermined set of potential wells, instead center of any model cell within the study area (or subsets of the study area) may be chosen as a monitoring site. The main limitation of the proposed method is that the only spatial patterns considered for peak concentration, and the time of the peak concentration, are those that are obtained from a relatively small set of model runs. The design of the network therefore relies heavily on having a robust groundwater model, from which plausible realization of plumes constrained by existing data can be obtained.

The remainder of this paper is organized as follows. Section 2 describes the details of the proposed methodology. Section 3 presents the application of the methodology for the optimal design of a monitoring network capable of robust prediction of peak concentration, and peak time resulting from a large-scale injection scheme. The major results from the application are presented and discussed in section 4 and the conclusions are presented in section 5.

## 2. Methods

There are three essential components for the optimal monitoring network design methodology proposed in this study. They are (i) the stochastic groundwater flow and transport model for simulating (and obtaining distributions for) the peak concentration and the time of peak concentration of the contaminant plume; (ii) dimension reduction of the spatial fields from (i) into spatial basis functions that define dominant spatial patterns; and (iii) identification of the optimal monitoring well locations and sampling times via stochastic optimization of a suitable objective function. Figure 1 depicts the key components of the method development of the proposed monitoring network design.

### 2.1. Stochastic Groundwater Flow and Transport Modeling

Calibration-constrained stochastic simulation approach known as Null-space Monte Carlo [Tonkin and Doherty, 2009] was used in this study to quantify the uncertainty in the contaminant concentration over space and time. The Null-space Monte Carlo method provides an efficient means of exploring predictive uncertainty by generating many different parameter fields all of which honor model calibration constraints.

Implementation of the Null-space Monte Carlo method requires the calibration of the model, resulting in the computation of a parameter field  $\mathbf{p}$  and a Jacobian matrix  $\mathbf{X}$ . The matrix  $\mathbf{X}$  comprises the first derivative of the model predictions with respect to the parameter field  $\mathbf{p}$ . A model calibrated using a highly parameterized approach (like pilot points in this study) can provide a parameter covariance matrix  $\mathbf{C}(\mathbf{p})$  that describes the spatial variability of the hydrologic properties. Random parameter fields  $\mathbf{p}_r$  can then be generated by using this parameter covariance matrix of innate parameter variability  $\mathbf{C}(\mathbf{p})$ . However, very few model runs using these randomly generated parameter fields will result in an acceptable value of the calibration objective function. The calibrated parameter field is then subtracted from the stochastically generated parameter field. The difference between the two ( $\mathbf{p}_r - \mathbf{p}$ ) is projected onto the calibration Null-space

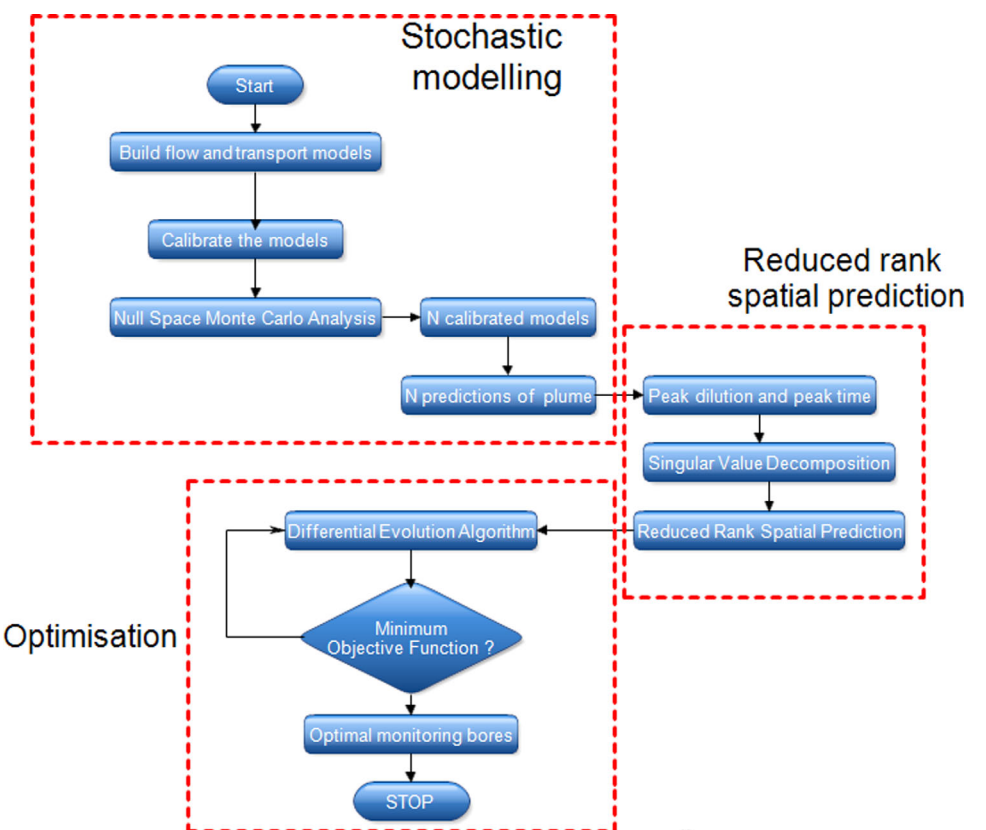


**Figure 1.** Flow diagram for the steps involved in the design of the monitoring well network. The first component is the stochastic modeling of groundwater flow and transport that results in an ensemble of predictions. The second component uses empirical orthogonal functions for reduced-rank prediction of the spatial fields and the third component uses the spatial predictions together with an optimization algorithm to optimize monitoring network design.

(i.e., onto the space of parameters that cannot be estimated based on the calibration data set). Then, the solution-space component of the stochastically generated parameter field is replaced by the parameter field arising from the initial calibration. This is achieved by undertaking the following steps [Doherty, 2012]:

1. Calibrate the model using available observation data and estimated the calibrated parameter field  $\underline{\mathbf{p}}$  and the Jacobian matrix  $\mathbf{J}$  pertaining to the sensitivity of the model predictions to the calibrated parameter field  $\underline{\mathbf{p}}$ .
2. Undertake singular value decomposition of  $\mathbf{Q}^{1/2}\mathbf{J}$ , where  $\mathbf{Q}$  is the observation weight matrix used for calibration which is based on the measurement uncertainty, using the formula:

$$\mathbf{Q}^{1/2}\mathbf{J} = \mathbf{U}\mathbf{S}\mathbf{V}^T \quad (1)$$

3. Generate a new random parameter vector  $\mathbf{p}_r$  using the parameter covariance matrix  $\mathbf{C}(\mathbf{p})$  and compute the difference  $\mathbf{p}_r - \underline{\mathbf{p}}$ .
4. Components of parameter differences encapsulated in  $\mathbf{p}_r - \underline{\mathbf{p}}$  that possess a nonzero projection onto the calibration solution space are removed by computing the projected parameter differences  $\mathbf{p}_d$  using the equation:

$$\mathbf{p}_d = \mathbf{V}_2 \mathbf{V}_2^T (\mathbf{p}_r - \underline{\mathbf{p}}) \quad (2)$$

where  $\mathbf{V}_2$  is obtained from  $\mathbf{V} = [\mathbf{V}_1 \ \mathbf{V}_2]$  and  $\mathbf{V}_2$  is an orthogonal matrix whose columns span the calibration Null-space.

5. A new set of parameter values is then produced by adding  $\mathbf{p}_d$  to  $\underline{\mathbf{p}}$ .

The advantage of this method is that the resulting parameter set would calibrate the model in case of models for which the predictions are linearly related to parameters, because the Null-space parameters do not affect the model outputs. In practice, the Null-space projection results in a model that is slightly out of

calibration because of model nonlinearity. But the model can easily be recalibrated by adjusting the solution-space parameter eigenvectors and eigenvalues until the calibration objective function falls below a user-specified level. This method is described in detail in *Tonkin and Doherty [2009]*.

### 2.1.1. Peak Concentration and Peak Time

Predictive simulations, using many parameter fields identified using Null-space Monte Carlo analysis, result in many, equally likely realizations of model predictions. The Null-space Monte Carlo method was used in this study to simulate equally likely realizations of the concentration of contaminant plumes originating from an injection well field. Consider that the numerical groundwater transport model simulates the concentration of a contaminant plume in an aquifer that has been spatially discretized into a finite difference grid. The optimal monitoring network design proposed in this study uses two different sets of spatial fields from the stochastic model simulations. The first spatial field comprises predicted peak concentration of the concentration plume simulated at  $p$  grid cells (pixels) of the groundwater flow and transport model. The peak concentration is computed as the maximum value of concentration in each finite difference cell of the model over the entire time period of simulation. The second spatial field comprises the time corresponding to the peak concentration.

### 2.2. Reduced-Rank Spatial Prediction Using Empirical Orthogonal Functions (EOFs)

Let  $G_{1,j}, \dots, G_{s,j}$  be a collection of  $s$  spatial fields output from the  $j$ th run of a stochastic model ( $j=1, 2, \dots, m$ ). In the present case study  $s = 2$  corresponding to two spatial fields of peak concentration and peak time obtained from groundwater model simulations. However, the method can be readily extended to include other number of spatial fields in the monitoring network design if desired.

For the  $i$ th output ( $i=1, \dots, s$ ) of the  $j$ th model run, the spatial field is comprised of  $p$  pixels obtained from  $p$  grid cells of the groundwater model, denoted

$$G_{i,j} = (g_{i,j,1}, \dots, g_{i,j,p}) \quad (3)$$

Let  $\mathbf{X} = (\mathbf{x}_1, \mathbf{x}_2, \dots, \mathbf{x}_m)$  be a matrix, whose column vectors are defined as

$$\mathbf{x}_j = (G_{1,j}, \dots, G_{s,j})^T \quad (4)$$

(i.e., the concatenated pixel values for all  $s$  spatial fields output from a single model run). Compute,

$$\mu_k = m^{-1} \sum_{j=1}^m X_{k,j} \quad (k=1, 2, \dots, ps) \quad (5)$$

and

$$\sigma_k = \left( m^{-1} \sum_{j=1}^m (X_{k,j} - \mu_k)^2 \right)^{1/2} \quad (6)$$

as the mean and standard deviation of the  $k$ th pixel over the  $m$  model runs. Collect these into three vectors as follows:

$$\tilde{\boldsymbol{\mu}} = (\mu_1, \dots, \mu_{ps})^T \quad (7)$$

$$\tilde{\boldsymbol{\sigma}} = (\sigma_1, \dots, \sigma_{ps})^T \quad (8)$$

$$\tilde{\boldsymbol{\sigma}}^{-1} = (1/\sigma_1, \dots, 1/\sigma_{ps})^T \quad (9)$$

Using these, we center and scale  $\mathbf{X}$  to create the matrix:

$$\mathbf{X}^* = (\mathbf{x}_1^*, \mathbf{x}_2^*, \dots, \mathbf{x}_m^*) \quad (10)$$

where

$$\mathbf{x}_j^* = \text{diag}(\tilde{\boldsymbol{\sigma}}^{-1})(\mathbf{x}_j - \tilde{\boldsymbol{\mu}}) \quad (11)$$

The aim herein is to find a relatively small set of basis functions through which the spatial patterns in the  $sp$  pixels of each model run can be well approximated. The main advantage and purpose of this component of the method is that the spatial basis functions can be used in conjunction with a global optimization

algorithm with much reduced computational cost for designing the optimal monitoring network. This modeling approach is often referred to as *dimension reduction* or *reduced-rank regression*. Dimension reduction is achieved by means of the Karhunen-Loève decomposition of a zero-mean stochastic process into a linear combination of orthogonal basis functions. For stochastic processes over discrete domains (such as the pixels of our model outputs), this decomposition is implemented by means of a singular value decomposition, applied to the matrix  $\mathbf{X}^*$ . The act of centering this matrix is used to ensure that the  $m$  model outputs can be reasonably considered realizations of a zero-mean stochastic process. Pixel-wise scaling can be used to ensure that all pixels in the spatial fields are given equal importance when formulating the spatial basis functions, regardless of differences in pixel magnitudes on the natural scale. In this application, we found pixel-wise scaling to have a negligible effect on our results, but we present the approach in its entirety, as this may be more useful in other settings.

Using a singular value decomposition of the matrix  $\mathbf{X}^*$ , let

$$\mathbf{X}^* = \mathbf{UDV}^T \quad (12)$$

where,

$$\mathbf{D} = \text{diag}(d_1, d_2, \dots, d_m) \quad (13)$$

For a monitoring design consisting of  $n$  locations, let  $d_{a_1}, \dots, d_{a_n}$  denote the  $n$  largest diagonal elements of  $\mathbf{D}$  (assuming  $n$  is not greater than the rank of  $\mathbf{X}^*$ ) and  $a_1, \dots, a_n$  be their indices along the diagonal. In the next step, construct a matrix of those spatial basis functions having the greatest ability to explain variability exhibited in  $\mathbf{X}^*$ , as

$$\mathbf{U}^* = (\mathbf{S}\mathbf{U}_{\cdot, a_1}, \dots, \mathbf{S}\mathbf{U}_{\cdot, a_n}) \quad (14)$$

where  $\mathbf{U}_{\cdot, a_i}$  represents column  $a_i$  of the matrix  $\mathbf{U}$  and

$$\mathbf{S} = \text{diag}(\tilde{\sigma}) \quad (15)$$

The columns of  $\mathbf{U}^*$  represent orthogonal multivariate spatial basis functions that account for dominant patterns of spatial variability observed in  $\mathbf{X}^*$  (and therefore in the  $s$  spatial fields output by the model). These orthogonal basis functions are commonly referred to as *empirical orthogonal functions* (EOFs) in fields such as meteorology and oceanography.

We wish to predict the pixel values in all  $s$  spatial fields given only  $n$  observations at identical pixel indices across all fields, henceforth denoted as

$$\mathbf{w} = (w_1, w_2, \dots, w_n) \quad (16)$$

where  $w_k \in \{1, 2, \dots, p\}$  and  $k \in \{1, 2, \dots, n\}$ . Assuming that model run  $j$  provides a true representation of the  $s$  spatial fields in nature, then the vector of field observations is defined as

$$\tilde{\mathbf{y}}_j = (g_{1,j,w_1}, g_{1,j,w_2}, \dots, g_{1,j,w_n}, \dots, g_{s,j,w_1}, g_{s,j,w_2}, \dots, g_{s,j,w_n})^T \quad (17)$$

Given the pixels at which observations are made, the corresponding basis function matrix at these locations is written as

$$\mathbf{U}_w^* = \left[ (U_{w_1, a_1}, \dots, U_{w_n, a_1})^T, \dots, (U_{w_1, a_n}, \dots, U_{w_n, a_n})^T \right] \quad (18)$$

and the corresponding values of  $\tilde{\mu}$  are written as

$$\tilde{\mu}_w = \left( \mu_{w_1}, \dots, \mu_{w_n}, \mu_{p+w_1}, \dots, \mu_{p+w_n}, \dots, \mu_{(s-1)p+w_1}, \dots, \mu_{(s-1)p+w_n} \right)^T \quad (19)$$

We assume that given the vector of observations,  $\mathbf{y}_j$ , the complete set of pixels for each of the  $s$  spatial fields can be approximated by first computing the least squares regression coefficient vector:

$$\hat{\beta}_j = \left( (\mathbf{U}_w^*)^T \mathbf{U}_w^* \right)^{-1} (\mathbf{U}_w^*)^T (\tilde{\mathbf{y}}_w - \tilde{\mu}_w) \quad (20)$$

and subsequently obtaining a prediction for all pixels in all spatial fields by computing

$$\tilde{\mathbf{x}}_j = \tilde{\boldsymbol{\mu}} + \mathbf{U}^* \hat{\boldsymbol{\beta}}_j \quad (21)$$

The pixel values for the first spatial field are contained in the subvector  $(\tilde{x}_1, \dots, \tilde{x}_p)$ , the second spatial field in the subvector  $(\tilde{x}_{p+1}, \dots, \tilde{x}_{2p})$ , and so forth.

### 2.3. Optimal Design of Monitoring Well Locations Via Differential Evolution

To determine the optimal locations of monitoring wells, we made use of  $m = 425$  runs of a stochastic groundwater model, we make the assumption that our groundwater model provides the best available characterization of the groundwater system and that each of the sets of stochastic model outputs could be considered a plausible and equally likely representation of the state of nature. The objective of the design is to find a set of  $n$  well locations, denoted  $\mathbf{w} = (w_1, w_2, \dots, w_n)^T$  amongst all possible well locations given by

$$W \equiv \{w_i \in \{1, 2, \dots, p\}^n : w_i \neq w_j \forall i, j \in \{1, \dots, n\}\} \quad (22)$$

Given  $m$  model runs, our aim is to solve the following optimization problem:

$$\mathbf{w}^* \equiv \operatorname{argmin}_{\mathbf{w} \in W} f(\mathbf{w} | \mathbf{X}) \quad (23)$$

The objective function  $f(\mathbf{w} | \mathbf{X})$  is a function of the well locations and its value is conditional on the matrix,  $\mathbf{X}$ , containing a representative sample of  $m$  possible model realizations. Herein, we define the objective function as

$$f(\mathbf{w} | \mathbf{X}) = \sum_{j=1}^m \sum_{k=1}^{sp} |(\tilde{\mathbf{x}}_j)_k - (\mathbf{x}_j)_k|^\rho \quad (24)$$

where  $(\tilde{\mathbf{x}}_j)_k$  denotes the  $k$ th element of the predicted vector where our observations are taken from model run  $j$  and  $(\mathbf{x}_j)_k$  denotes the  $k$ th element of the vector from model run  $j$ .

In doing so, the optimal monitoring locations identified are robust to different possible outcomes simulated using the stochastic model runs and result in a good spatial prediction for the  $s$  fields of interest, regardless of which one of the  $m$  possibilities turned out to be the true representation of nature.

We solve the global optimization problem above using a stochastic optimization procedure known as Differential Evolution [Storn and Price, 1997] which we implement using the DEoptim package [Mullen et al., 2011] for the R statistical programming language [R Core Team, 2015]. In developing this approach, we examined the effects of setting  $\rho = 1$  and  $\rho = 2$ , where the former was expected to result in less influence from outlying pixels than the latter. However, in the presented application, we found negligible difference in the results from these two parameterizations and we therefore adopt  $\rho = 2$  herein. The Differential Evolution algorithm we employed is outlined in the following steps:

1. Set  $T = 500$  as the number of iterations of the algorithm and  $t = 1$  as the current step.
2. Set  $P = 10n$  (as the number of candidate wells to randomly generate at each iteration, where recall that  $n$  is the number of monitoring wells we require),  $C = 0.5$  (as the crossover probability, which allows for the generation of new well locations) and  $F = 0.8$  (as the differential weighting factor in the generation of new well locations).
3. Initialize  $P$  vectors, denoted  $\tilde{\mathbf{w}}_i$  ( $i = 1, \dots, P$ ), with each vector containing the  $n$  pixel indices for a candidate set of well locations. Begin by distributing the locations within each vector uniformly at random over the study region.
4. If  $t < T$ , then repeat the following steps, otherwise go to step 6:
  1. For each vector of candidate wells  $\tilde{\mathbf{w}}_i$  in the set  $\{\tilde{\mathbf{w}}_1, \dots, \tilde{\mathbf{w}}_P\}$ , perform the following:
    1. Set  $\mathbf{y}_i = \tilde{\mathbf{w}}_i$ .
    2. Let  $(\tilde{\mathbf{w}}_{i,1}, \tilde{\mathbf{w}}_{i,2}, \tilde{\mathbf{w}}_{i,3})$  be a sample without replacement from  $\{\tilde{\mathbf{w}}_1, \dots, \tilde{\mathbf{w}}_P\}$ , with  $\tilde{\mathbf{w}}_{i,k} \neq \tilde{\mathbf{w}}_i$  (for  $k = 1, 2, 3$ ) and ordered so that  $f(\tilde{\mathbf{w}}_{i,1} | \mathbf{X}) \leq f(\tilde{\mathbf{w}}_{i,2} | \mathbf{X}) \leq f(\tilde{\mathbf{w}}_{i,3} | \mathbf{X})$ .
    3. Sample one well index,  $R_i$ , from the set  $\{1, \dots, n\}$  with equal probability.
    4. For each well location  $j$  in  $\{1, \dots, n\}$ , do the following:
      1. Let  $U_j \sim U(0, 1)$ .
      2. If  $j = R_i$  or  $U_j < C$ , then modify the  $j$ th element of  $\mathbf{y}_i$  according to  $y_{i,j} = \tilde{w}_{i,1,j} + F(\tilde{w}_{i,2,j} - \tilde{w}_{i,3,j})$ . Here  $\tilde{w}_{i,1,j}$  denotes the  $j$ th element of  $\tilde{\mathbf{w}}_{i,1}$ .
  - Recall  $f(\cdot)$  is the objective function defined previously. If  $f(\mathbf{y}_i | \mathbf{X}) \leq f(\tilde{\mathbf{w}}_i | \mathbf{X})$ , then set  $\tilde{\mathbf{w}}_i = \mathbf{y}_i$ .

5. Set  $t$  equal to  $t + 1$  and go to step 4.
6. Return the  $\tilde{\mathbf{w}}_t$  that has the smallest objective function  $f(\tilde{\mathbf{w}}_t | \mathbf{X})$ .

### 3. Case Study

The method was applied to a theoretical case study that is based on a realistic injection well field in the Surat Basin in Australia, where CSG production has commenced on a commercial scale. The following assumptions were made in the application of the proposed method to this case study: (i) Some hydrogeological site information is available for the development and calibration of groundwater flow and transport models for the study area and (ii) it was assumed that the sole sources of uncertainty surrounding the contaminant plume migration are the uncertainty in the hydraulic conductivity values, porosity, longitudinal dispersivity, and lateral boundary conditions of the model. It should be noted that there are other factors that can have a significant influence on prediction uncertainty. This can include model conceptual uncertainty (e.g., uncertainty of the hydrostratigraphy and number of model layers), uncertainty of model inputs (e.g., injection rates) and uncertainty of other parameters (e.g., parameters of the variogram used to describe heterogeneity). These were not considered in the current proof-of-concept case study.

It is estimated that CSG production will result in peak extraction of about 100 GL of water per year [Queensland Government, 2016]. Major CSG proponents operating in this basin are considering reinjection of produced water, after treatment, for beneficial use. In this study we considered one reinjection schemes by which about 22 ML/d of reverse osmosis treated water will be injected into a confined sandstone aquifer in the Surat Basin. The scenario simulated considered a constant rate of injection over a stress period of 1 month, but varies from one stress period to another. The total injection rate was apportioned to 12 wells based on estimated hydraulic conductivity at the locations. The sandstone formation is a regional fresh water aquifer in the Surat Basin. A rectangular block with an area of 225 km<sup>2</sup> which encompasses the locations of 12 proposed injection wells was selected for building the groundwater flow and transport models using MODFLOW and MT3D codes. The model area was discretized into cells of variable sizes ranging between 50 and 225 m with the finer discretization closer to the injection wells. Vertically, the model was discretized into two layers. The upper layer corresponded to a less porous zone of the sandstone formation. The injection wells are considered to be screened in the lower layer.

#### 3.1. Model Calibration

The data available for model calibration comprised head observations from pump tests and existing monitoring wells, as well as head and tracer concentration data from injection trials carried out in one of the monitoring wells. Calibration of the model was achieved by varying the flow and transport parameters as spatially varying fields. Automated calibration of the model was achieved using the model inversion tool PEST. The PEST pilot point functionality was used to implement heterogeneous hydraulic property fields. By using this approach, hydraulic property values at the pilot points are varied during calibration to match predicted heads and concentrations to corresponding observations. The hydraulic properties of model cells other than the pilot points are interpolated from the pilot points using Ordinary Kriging with a semivariogram that used an exponential correlation function. Sufficient amount of data was lacking to estimate the parameters of the variogram. Considering the large uncertainty in the hydraulic properties of the formation a conservative approach was used in characterizing spatial variability. An exponential variogram with a nugget value of 1.5 and sill of 3.0 in log domain was used. Relatively large value of nugget was used to conservatively estimate uncertainty in the variability of model parameters given limited data available to inform the choice of these parameters. Limited hydrogeological investigations conducted near the well field indicated large variability of hydraulic conductivity across locations but the formation itself is regionally continuous. The correlation length used was 10 km given the regional nature of the geologic formation.

Horizontal and vertical hydraulic conductivities, and the specific storage for each model layer, were parameterized using 25 pilot points each. Similarly, two additional sets of 25 pilot points each were used for parameterizing porosity and dispersivity spatially for each layer. In addition to these, the lateral boundary of the model was defined as head dependent flux boundary, and the conductance of these boundaries were parameterized using a set of 32 pilot points. No-flow boundary was used for the bottom and spatially variable recharge boundary was used for the model top.

Pump tests were conducted for two wells in the injection well field, and injection trials and tracer tests were conducted in one well. The injection trial was conducted over a period of 6 months. The resulting pressure changes were monitored in both wells. The tracer concentrations were monitored at the well where the push-pull test was conducted. The pressure changes within the model domain resulting from the proposed injection scheme also was simulated by another regional scale model that was calibrated to head observations from larger number of regional monitoring bores. The pressure changes simulated by this regional scale model at nine locations in the well were used as additional constraints for calibrating the flow model. Thus, model calibration used four different groups of observations comprising the steady state head observations, transient head observations from pump tests and injection trials, the information provided by the tracer tests and simulated transient head constraints from the regional model simulations. A total of 3400 observations were present across these four groups. The observations were normalized using weights in the objective function to ensure that the contribution to the total objective function from these four groups is equal. Minimization of the least square deviation between the observations and predictions was used as the calibration objective function in PEST.

### 3.2. Injection Scenario

An injection scenario proposed by the coal seam gas proponent was considered for the purpose-built long-term monitoring network design. The scenario comprised an average injection rate of 22.1 ML/d over a period of 22 years. The constant monthly injection rate would be distributed among 12 injection wells in proportion to the estimated transmissivity at these well locations. The injection rate varied from month to month based on the estimates of coal seam gas water production during each time period. The primary risk of such a large-scale injection scheme is the potential of mobilization of geochemical contaminants from the aquifer. In order to predict the advection-dispersion transport of such potential contaminants and use this information for the design of monitoring wells, we considered source strength of 1 mg/L at each well. Unit source strength was used so that the simulated concentration at any location will indicate the concentration. A detailed local scale modeling was undertaken to closely examine the reactive transport processes triggered by the mixing of injected water with the native water and minerals in a separate project that was linked to the present study. However, the major focus of this paper is limited to the design of optimal monitoring wells using the conservative transport simulations carried out for the well field.

### 3.3. Stochastic Simulation of Concentration

Calibration of the model using the PEST [Doherty, 2012] resulted in a calibrated parameter set  $\underline{p}$ . In this study,  $\underline{p}$  is a vector of all the model parameters and is informed by 3400 observations. Unique estimation of heterogeneous groundwater transport parameters was challenged by the absence of tracer data from multiple wells. However, parameterizing these properties with 25 pilot points helped to explore parameter uncertainty on transport predictions and subsequently account for uncertainty in the design of monitoring wells. Thus, parameterizing the model with large number of parameters was intended to explore the model prediction uncertainty to inform the monitoring network design rather than accurate estimation of these parameters. After calibrating the model, the Null-space Monte Carlo method was employed to identify many parameter combinations which were equally good in calibrating the model. A total of 425 sets of the parameters were identified and model predictive uncertainty was explored by running the injection scenario for each parameter set. Model simulations with all the 425 parameter sets resulted in equally likely realizations of potential plumes. Peak concentration and peak time matrices were then obtained as described in section 2.

### 3.4. Sampling Location and Time Selection

All simulated plumes represented equally likely realizations of the contaminant plume informed by the available observations. We determined data-worth to be maximized at locations that minimized predictive error across the spatial domain, regardless of which simulated plume turned out to be the true state of nature. This was achieved by locating the monitoring wells so that predictions from the reduced-rank spatial prediction of the peak concentrations and peak times had the least deviating from the stochastic numerical model simulations. By using the monitored concentrations at these locations in the reduced-rank spatial prediction, we ensure the best estimate of the plume for the available level of information.

The expected value and the distribution of the peak concentration and peak time at the designed monitoring locations are known from the Null-space Monte Carlo simulations. A threshold for noncompliance can

be easily determined using the concentration distribution. For example, suppose we used the 95th percentile of the peak concentration from the simulations to define the limit of undesirably high contamination at a monitoring location. Monitoring the concentration at the designed locations and using it with the reduced-rank spatial prediction allows us to estimate the peak concentrations over the entire well field. However, if the concentration measured at the monitoring location exceeds this set limit, it implies that peak concentration is high in the range of the values we expect to see, and that remedial measures might be required. Further, the model can be recalibrated with this updated information and whole procedure can be repeated to update the system state.

We assume that the monitoring frequency can be as small as monthly equal to the resolution of the stress periods used in the modeling. Incorporation of peak time in the monitoring network design has the advantage that it provides the best estimate of the time at which peak concentration occurs at any point in the well field. In practice this is could be useful for sequential drilling of the monitoring wells. At each location, the 425 model runs provide a distribution for when the peak should occur and so drilling could be staged in time in order to have each well in place by the time the peak should occur. As wells are drilled and more data are acquired, we might expect to obtain better predictions of the peak time, which would further

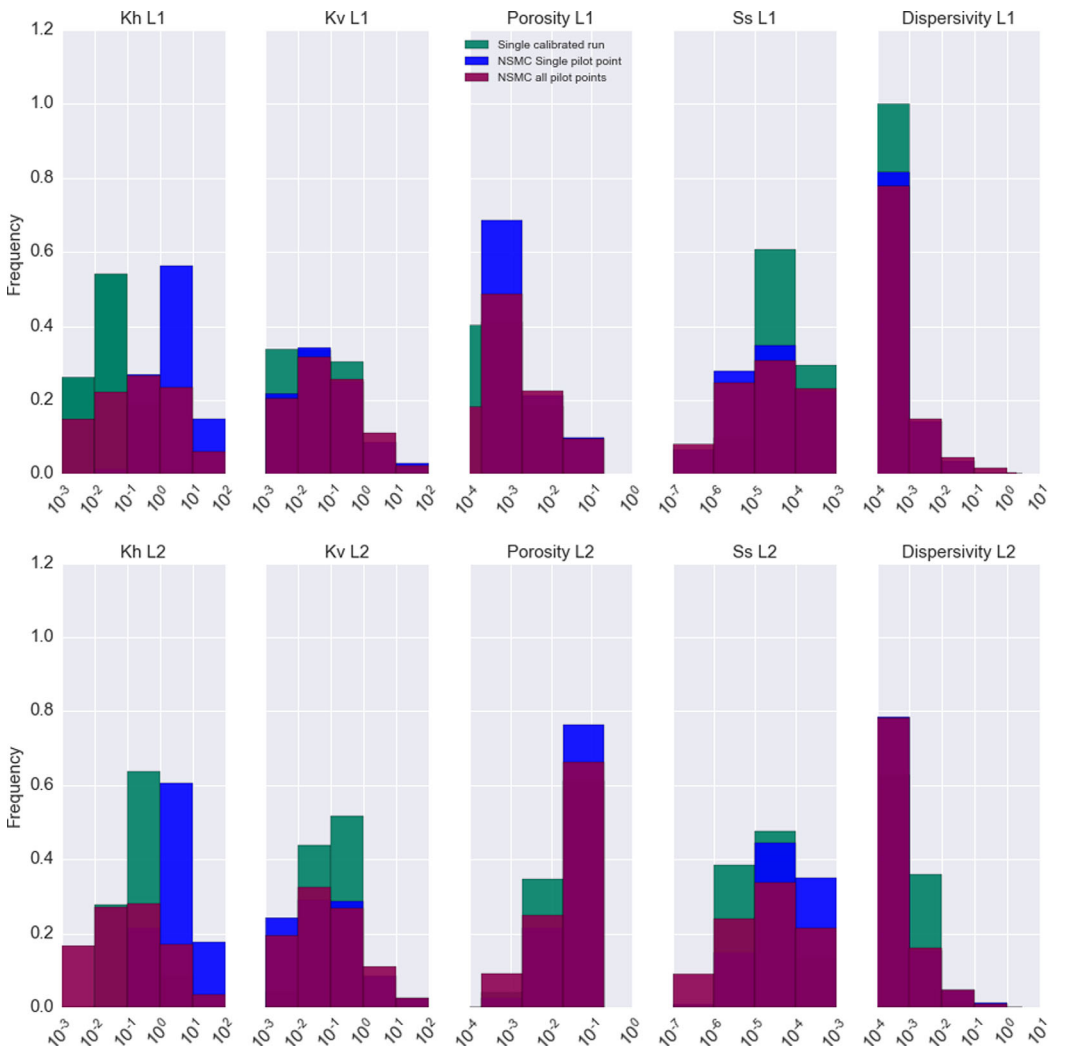


**Figure 2.** Distribution of hydraulic property parameters—horizontal hydraulic conductivity ( $\text{m/d}$ ), vertical hydraulic conductivity ( $\text{m/d}$ ), porosity and specific storage, and longitudinal dispersivity ( $\text{m}$ ) for the two model layers. Each subplot shows distribution of one hydraulic property obtained from (a) one single calibrated model cells, (b) distribution of hydraulic property at one pilot point location across 425 simulations, and (c) distribution of hydraulic property at all pilot points across 425 simulations.

inform the times at which the additional wells should be drilled and data regarding peak concentration and peak time collected.

## 4. Results

### 4.1. Null-Space Monte Carlo Analysis

The distributions of spatially variable hydraulic properties obtained from the Null-space Monte Carlo simulation are shown in Figure 2. The figure shows (a) the distribution of properties across the model domain obtained from one single calibration run, (b) the distribution of parameters at one pilot point obtained from the Null-space Monte Carlo simulation, and (c) distribution of properties across all pilot points obtained from the Null-space Monte Carlo simulation.

The confidence in the parameter distribution obtained from any single calibration exercise depends on the information content of the observations used for calibrating the model. For example, groundwater head observations from multiple well locations within the well field provided useful information to constrain the horizontal hydraulic conductivity of the sandstone formation. On the other hand, tracer injection push-pull tests provided only limited information to constrain the spatial distribution of dispersivity parameters across the well field. This resulted in large uncertainty in the values of model parameters. For parameters like dispersivity, there can be a discrepancy between the scale at which parameters are observed and modeled. For example, observations may exist at wells (points in space) but are represented over large geographical areas in the model. Uncertainty in the values of hydraulic parameters results in large predictive uncertainty, and this was explored using Null-space Monte Carlo simulations. Null-space Monte Carlo simulations resulted in a wide range of values obtained for each hydraulic property as shown in Figure 2. This reflects the large uncertainty in the estimated values of these properties. Figure 2 also shows that the calibrated parameter value at each pilot point also varies significantly across multiple calibration runs.

A total of 425 simulations of the groundwater flow and transport model was undertaken to explore the uncertainty in the hydraulic properties and boundary conditions. Given that the transport predictions were

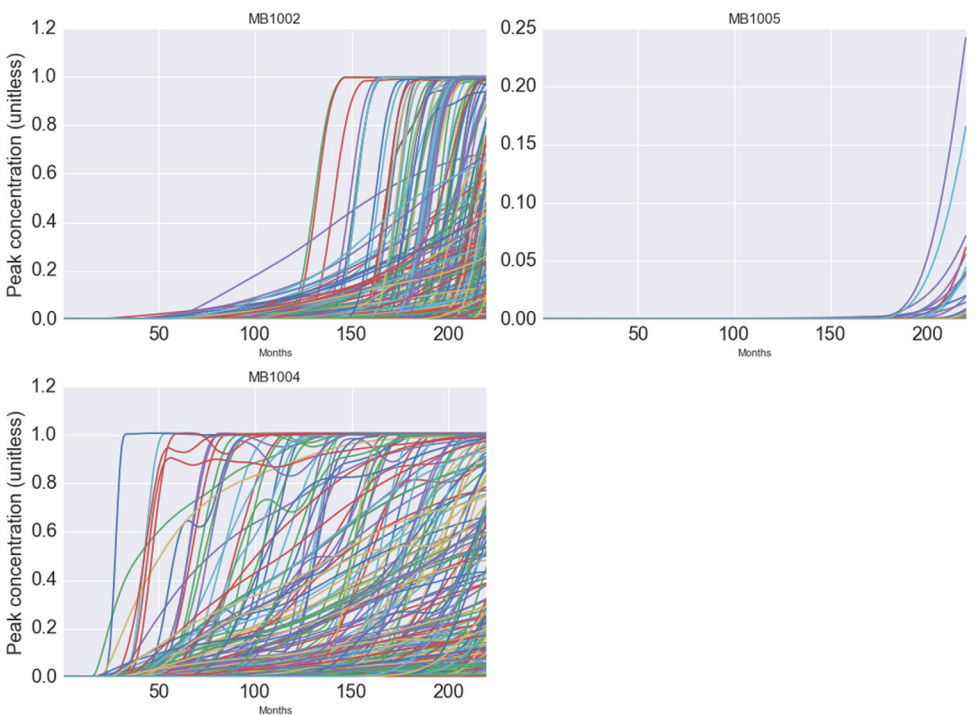


**Figure 3.** Predicted break-through of concentration at three monitoring wells. MB1004 is the monitoring well closest to the well field and is approximately at equal distance from three injection wells. MB1002 and MB1005 are located farther and concentration break-through in these wells take longer.

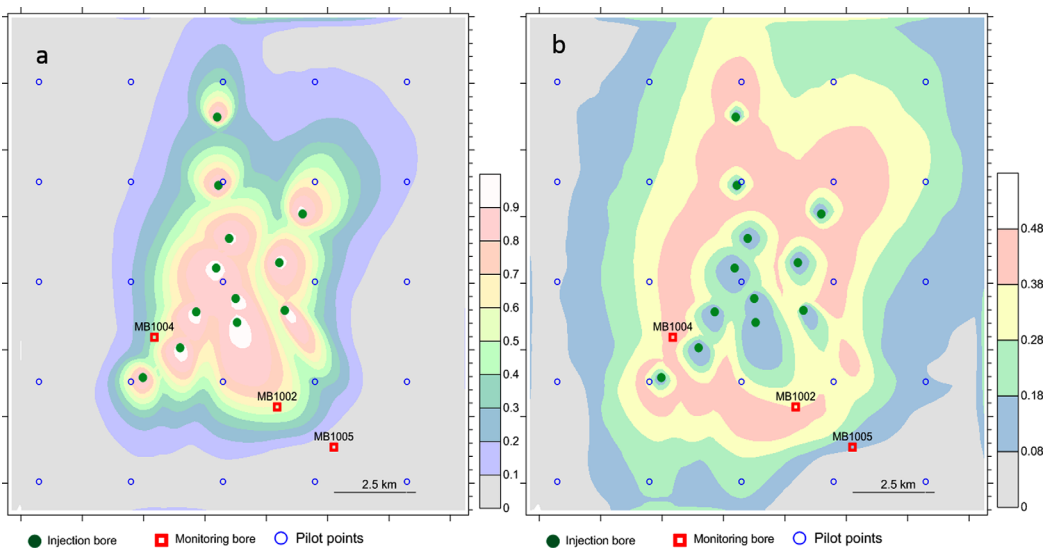


**Figure 4.** (a) Mean and (b) variance of the simulated peak concentration (unitless) from the Null-space Monte Carlo. The mean and variance of peak concentration were computed from 425 predictive runs of the flow and transport model by using the parameter fields obtained from the Null-space Monte Carlo.

informed by the observations from injection tracer tests in only one well, there was substantial uncertainty in the prediction of concentration in the well field. Examples of predicted concentration break-through curves at the three locations for 220 months since the start of injection is shown in Figure 3. The location of the three monitoring bores MB1002, MB1004, and MB1005 with respect to the injection wells are shown in Figures 4 and 5.

It is evident from these two plots that the predictive uncertainty is large. This is primarily because the information content from the available observations—pump tests and tracer tests and regional head observations are insufficient to constrain the spatial variability of heterogeneous fields of hydraulic conductivity, porosity and dispersivity parameters used in the model. Although these simulations are least useful in predicting the break-through curves at any specific location, it gave useful information for the design of monitoring wells for the long-term monitoring of water quality in the injection well field. For example, it can be

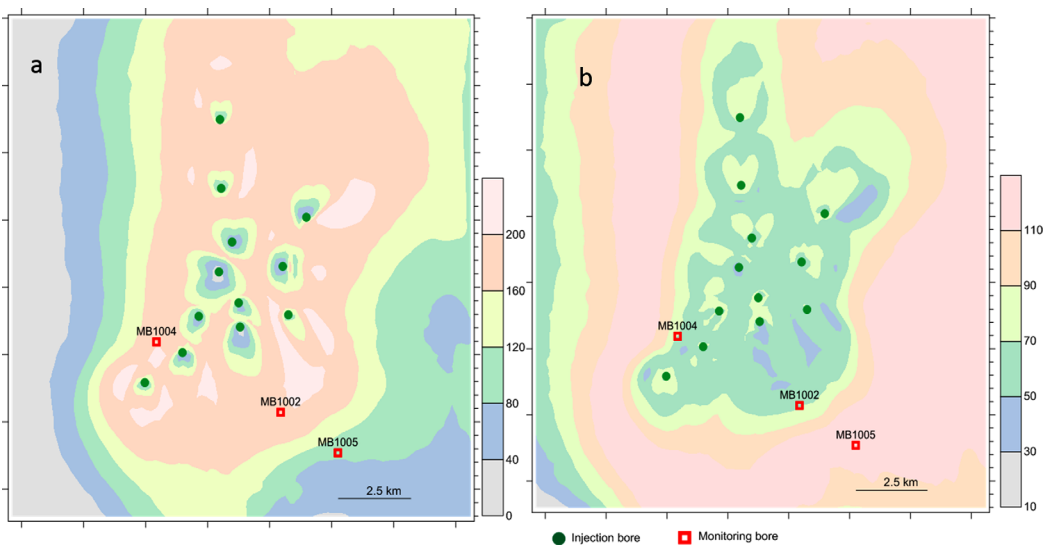


**Figure 5.** (a) Mean and (b) variance of the simulated peak time (months) from the Null-space Monte Carlo. The mean and variance of peak time were computed from 425 predictive runs of the flow and transport model by using the parameter fields obtained from the Null-space Monte Carlo.

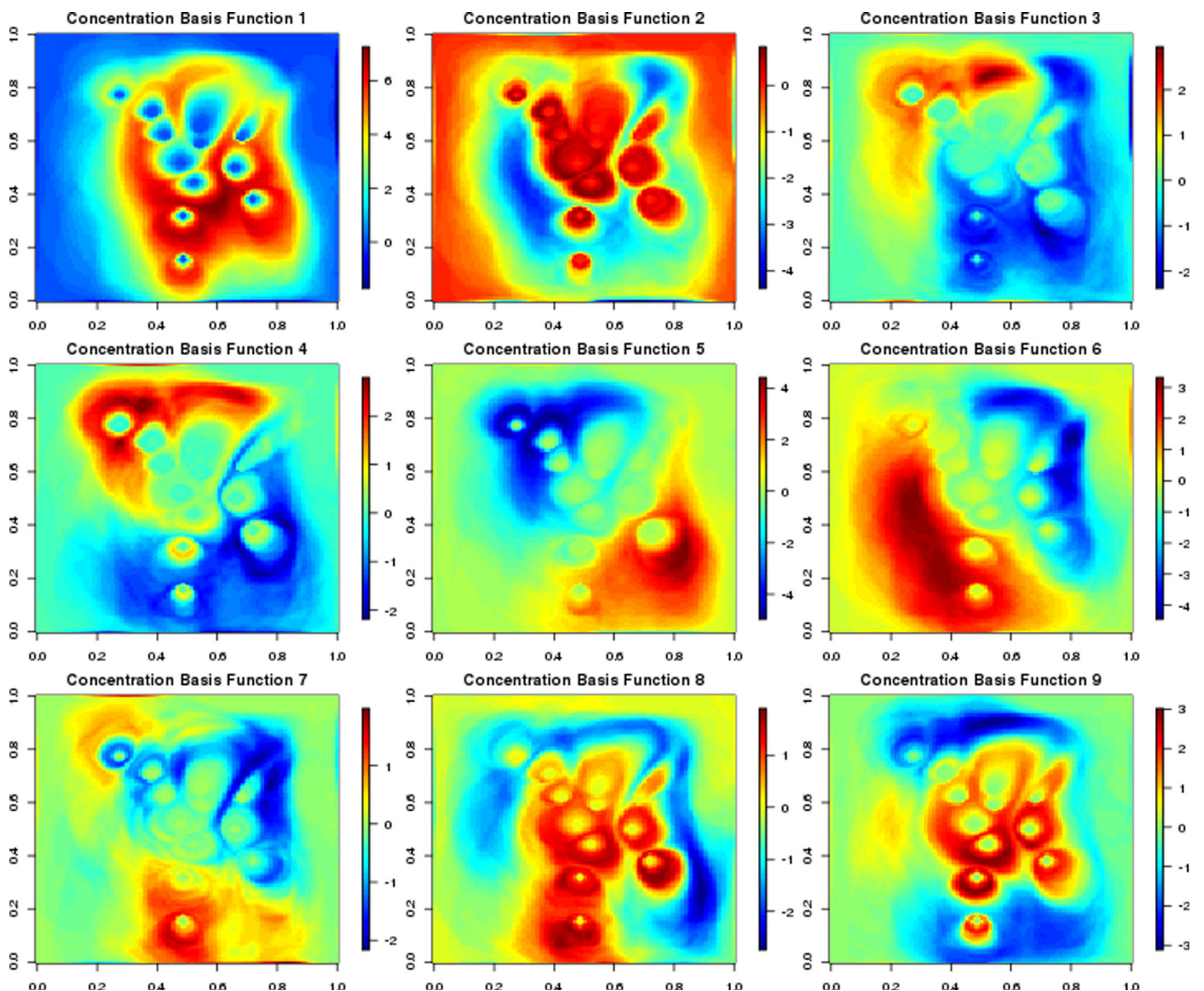


**Figure 6.** Spatial basis functions for peak concentration (unitless) The subplots show the dominant nine empirical orthogonal functions that explain the greatest proportion of variability in the ensemble flow and transport model runs.

inferred from Figure 3a that it is very unlikely that the peak concentration occurring at the monitoring well MB1002 will occur within the first few years of the commencement of injection. On the other hand, MB1004 (Figure 3c) which is closer to an injection well may reach the peak concentration even within the first few years. And, the location MB1005 may not monitor a water quality change for many years after the start of the injection (Figure 3b). To aid interpretation of Figure 3, the mean and variance of the predicted peak concentration and peak time across the 425 simulations, along with the locations of the injection wells and monitoring bores are given in Figures 4 and 5, respectively. Availability of this kind of information is very useful for evaluating the probability of the occurrence of peak concentration and peak time at all the locations within the model grid to use that information about when and where to monitor so as to obtain maximum data-worth and design the monitoring network accordingly. It may be noted from Figure 4b that the prediction uncertainty is least in the immediate vicinity of the wells and then again along the periphery of the plume where the peak concentration decreases to zero. Between these ranges, uncertainty in the estimation of the peak concentration gradually increases and then decreases again. This readily tells us that an efficient monitoring network should be able to monitor peak concentrations at locations distributed across the region.

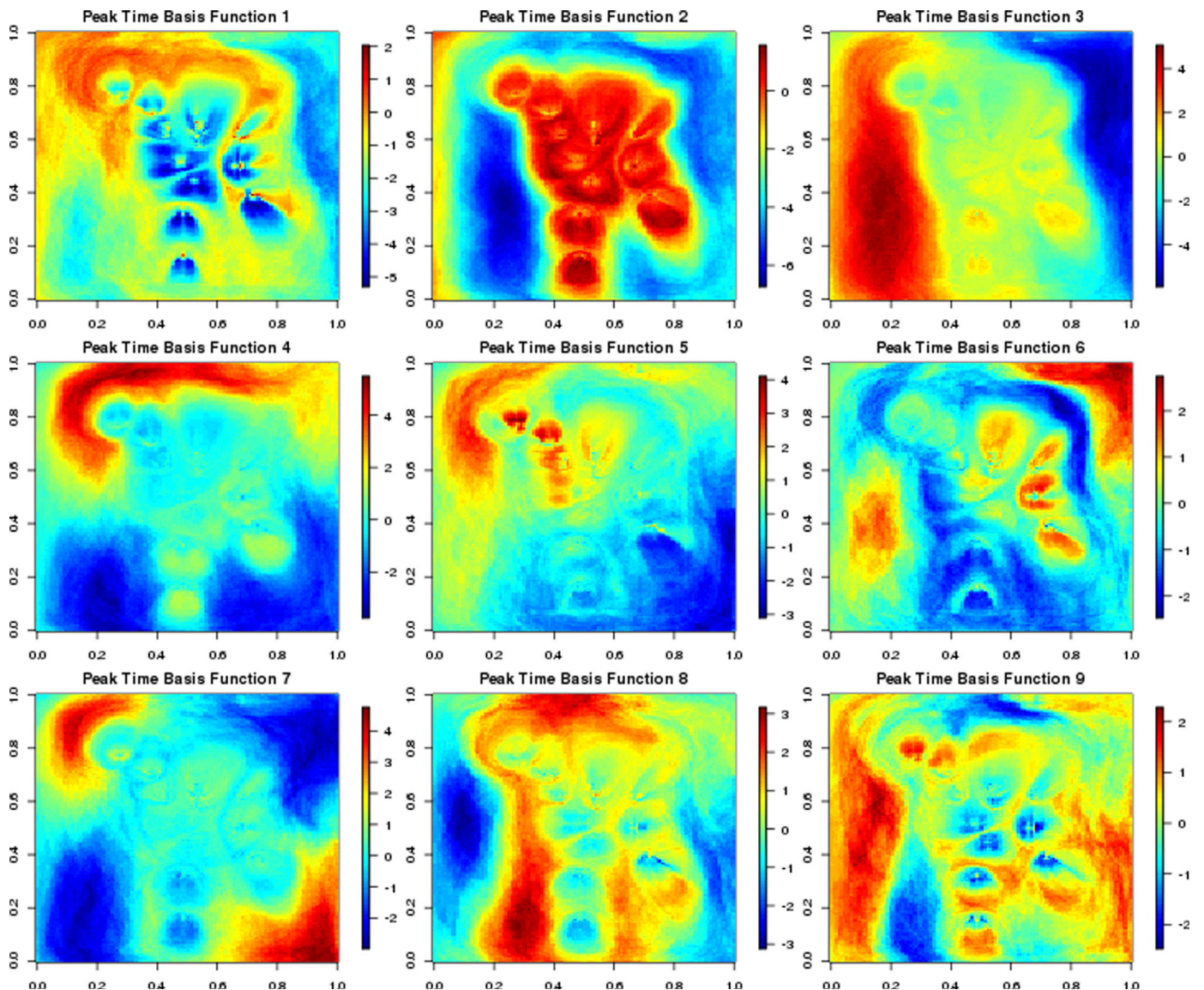


**Figure 7.** Spatial basis functions for peak time (normalized, unitless). The subplots show the dominant nine empirical orthogonal functions that explain the greatest proportion of variability in the ensemble flow and transport model runs.

#### 4.2. Spatial Basis Functions

Our method for interpolating the spatial fields of peak concentration and peak time relies upon identifying a collection of orthogonal spatial basis functions known as empirical orthogonal functions (EOFs). Figures 6 and 7 show the dominant nine EOFs (i.e., the nine left singular vectors from the singular value decomposition that have the largest singular values), these explain the greatest proportion of the variability in the ensemble of stochastic groundwater model runs. While each basis function for peak concentration and peak time has been presented separately, it is important to recognize that each basis function is actually over both peak concentration and time (i.e., the  $i$ th basis function is actually a vector containing all of the pixels from concentration basis function  $i$  and peak time basis function  $i$ ). In essence, each basis function provides the dominant orthogonal patterns in a multivariate spatial field.

#### 4.3. Optimal Monitoring Wells

We found our methodology to be robust in its ability to infer spatial fields of peak concentration and peak time from a relatively small number of monitoring wells for a diverse range of possible future states of nature, as represented by prediction variance in Figure 4b. For illustration purposes, Figures 8 and 9 show a

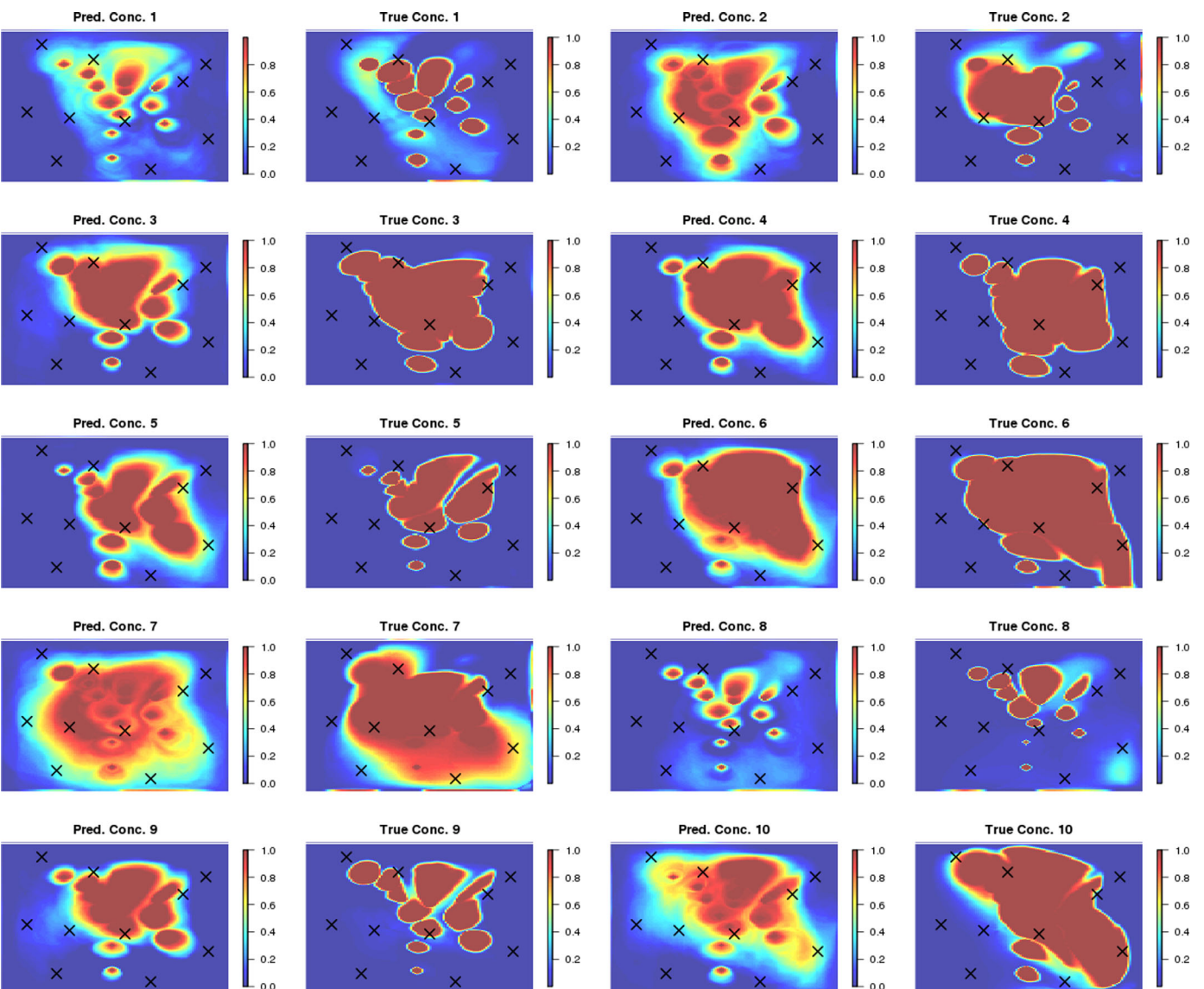


**Figure 8.** A comparison of the predicted and (assumed) true peak concentrations (unitless and normalized by dividing by the largest value in the spatial field) for a selection of ten model simulations. Crosses show the optimal locations of the monitoring wells in model layer 2.

sample of 10 randomly selected groundwater model runs that were each taken as the true state of nature, and the predicted spatial fields that our monitoring network and methods of prediction resulted in under these scenarios. It may be noted that the plumes we see in the plots are not any snapshot in time, but they show the peak concentration at any location over the 264 months simulation period. It is apparent that there is substantial variation in the spatial patterns that could be observed in reality, and our method is effective at predicting a wide range of these from a small number of monitoring wells. In reconstructing these spatial patterns, we assumed that the observation at the monitoring wells was equal to the truth (depicted) plus an additional measurement error of  $\pm 5\%$ .

Because Figures 8 and 9 only show a selection of ten such outcomes, we also present a summary of the errors and biases of our interpolation approach compared to each possible truth (i.e., each model run). Tables 1 and 2 show the mean squared error (MSE), mean absolute error (MAE) and the statistical bias (the average difference between the prediction and the truth) of our prediction method, computed over the pixels for each predicted spatial field. Quantiles and means of each of these statistics were computed for MSE, MAE and bias and show the variability in these quantities over the 425 simulations. In Figure 10, we also

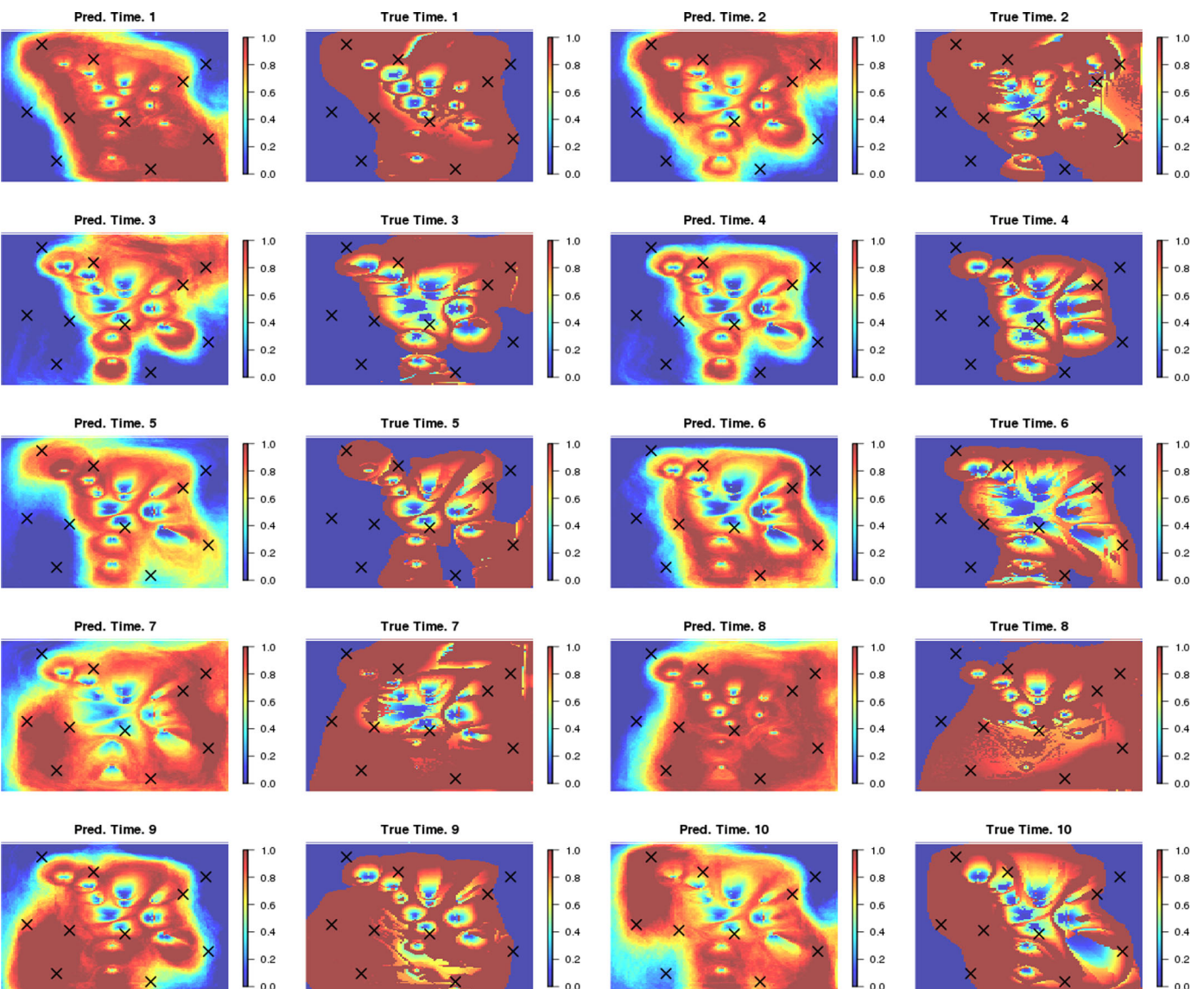


**Figure 9.** A comparison of the predicted and (assumed) true peak times (unitless) and normalized by dividing by the largest value in the spatial field for a selection of ten model simulations. Crosses show the optimal locations of the monitoring wells for layer 2.

present the distributions of pixel-wise errors across all 425 simulations when predicting normalized peak concentration and normalized peak time (both unitless), noting that both of these distributions show a heavy concentration of mass around zero error (i.e., good predictive accuracy).

Overall, bias across every possible outcome (model run) is negligible and error statistics are low, reinforcing that the results observed in Figures 8 and 9 are not anomalous and that the method and monitoring locations are robust to many possible future states of the groundwater system. The most obvious deficiency of the predictions arising from our approach is the errors that occur at step-like transitions from very high to very low values in the peak concentration and peak time surfaces. Our predictions have a tendency to

**Table 1.** Distributional Properties of Error Statistics Across the 425 Peak Concentration (Normalized and Unitless) Model Outputs

	5th P'tile	25th P'tile	Median	75th P'tile	95th P'tile	Mean
Mean squared error (MSE)	1.755E-2	2.655E-2	3.953E-2	5.278E-2	7.464E-2	4.161E-2
Mean absolute error (MAE)	7.032E-2	9.246E-2	0.1089	0.1330	0.1682	0.1140
Bias	-5.882E-2	-2.057E-2	8.133E-3	3.492E-2	6.551E-2	6.436E-3

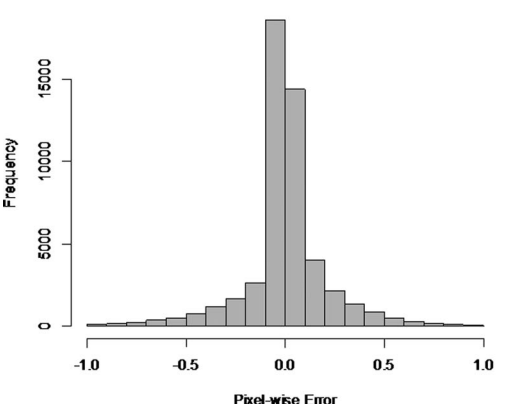
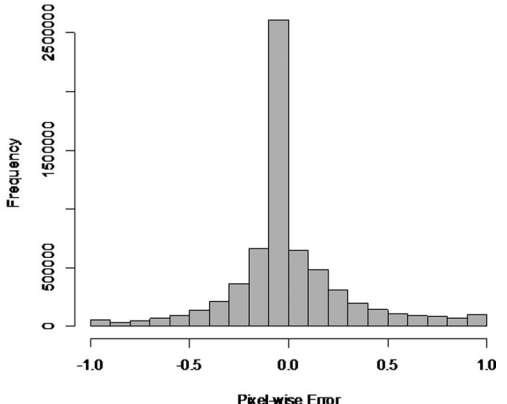
**Table 2.** Distributional Properties of Error Statistics Across the 425 Peak Time (Normalized and Unitless) Model Outputs

	5th P'tile	25th P'tile	Median	75th P'tile	95th P'tile	Mean
Mean squared error (MSE)	4.594E-2	6.194E-2	7.630E-2	9.343E-2	0.1253	7.975E-2
Mean absolute error (MAE)	0.1270	0.1536	0.1751	0.1985	0.2390	0.1776
Bias	-9.317E-2	-3.209E-2	5.980E-3	4.092E-2	9.166E-2	3.363E-3

smooth over these sharp transitions. The error statistics reported in Tables 1 and 2 could be used by regulators to have some idea of the magnitude of errors that might be encountered at these transitions.

Optimal locations for 10 monitoring wells identified using the proposed methodology are shown in Figures 8 and 9. It is notable that the optimal monitoring locations identified have good spatial coverage. It may be noted from comparisons of Figures (8 and 9), and 4, that the identified monitoring well locations cover the entire range of expected peak concentrations and peak times for the well field. This clearly indicates that the designed network will be monitoring a wide range of values of peak concentration and peak time, enabling reasonable estimates for the full range of these quantities within the plume.

There are some useful insights into groundwater monitoring that can be gleaned from Figures 8 and 9, particularly when the monitoring well locations are compared to the contours in Figure 4, showing the expected value of the peak concentration at any location within the well field based on the stochastic simulations. The monitoring wells closer to the well field will monitor higher values of peak concentration and at relatively earlier periods of the plume movement. For example, the monitoring well located toward the center of the well field is very close to the injection wells. Such monitoring wells are useful for monitoring at the “point of discharge” and ensure a preventive approach with a tighter control of the discharge quality [National Water Quality Management Strategy, 2014]. The “point of discharge” monitoring wells are useful to detect any unexpected changes in water quality near the injection field resulting from geochemical mobilization or other processes. For a comprehensive monitoring of compliance these “point of discharge” monitoring wells should be used in conjunction with monitoring wells at the boundaries of the concentration plume. It is also readily observable that some of the monitoring wells identified using our proposed approach are located along the boundaries where the peak concentration is tending toward the background concentrations. It should be noted that drilling monitoring wells at locations close to the boundaries may not be ideal if the objective of monitoring is mass estimation. However, from compliance monitoring point of view, monitoring the peak concentrations near the concentration boundaries is very important for avoiding environmental and health risks. The National Water Quality Management Strategy [2014] refers to this kind of monitoring as “verification” monitoring. Verification monitoring at the edges of the plume boundary is also required as evidence of effective contamination management for regulators. The National Water Quality Management Strategy [2014] highlights that “point of discharge” monitoring should be combined with “verification monitoring” near the edges of plume boundary within the aquifer, to confirm the accuracy of assumptions regarding plume movement.

**Normalised Peak Concentration Predictions****Normalised Peak Time Predictions****Figure 10.** Histograms of prediction errors for each pixel across all 425 simulations for normalized peak time (unitless) and normalized peak concentration (unitless) using the 10 monitoring wells identified.

#### 4.4. Integrated Space-Time Monitoring

The proposed monitoring network design approach integrates spatial and temporal monitoring objectives in one single objective function. While the optimization focuses on identifying the spatial locations for monitoring wells, it does so while ensuring that the time of the peak concentration field can be reliably estimated. Our use of multivariate EOFs would also enable the incorporation of other different types of variables in the monitoring network design if so desired. A comprehensive space-time monitoring design can be undertaken, using approaches like ensemble Kalman filter. However, such an approach would require the inversion of the covariance matrix corresponding to the space-time concentration vector at each step of the optimization algorithm. This adds to the computational complexity of such optimization algorithms, since the inversion is an operation of  $O(n^3)$  complexity. Often, the allowable monitoring locations are constrained or preselected in order to avoid prohibitive model run times while using such approaches [Herrera and Pinder, 2005]. In the proposed, simpler approach, the EOFs are used to reduce the dimensionality of the spatial field that is being modeled. This makes our approach computationally attractive and allows us to consider all finite difference cells in the numerical model as candidate monitoring sites instead of just a subset. Thus, in our case study, 15,222 locations were considered as potential monitoring wells for reliably predicting the concentration field and the times at which peak concentration occurs. The conventional Kalman filter based approach to design would have the computational burden of inverting a  $118 \times 129 \times 264$  matrix during each iteration of the optimization routine.

While our methods are presented for design of a static monitoring network design, the approach could be adapted for sequential design of monitoring networks. Under such a strategy, a 10 well monitoring network could be designed (perhaps one well at a time) and as data are collected, this information would be used to adjust: (i) the flow and transport modeling; (ii) the basis functions used (by consequence of updating (i)); and (iii) the optimal positions of the remaining, undrilled wells. This, and software to undertake such monitoring design is a subject of future research.

### 5. Conclusions

A novel method is proposed for the design of observation well network for optimal monitoring of groundwater quality compliance. The method is based on stochastic simulation of groundwater flow and transport to account for prediction uncertainty in the monitoring network design. Predictions from the stochastic simulations are used to identify a small number of multivariate, spatial basis functions that can be used to predict spatial fields of peak concentration and peak time from observations of these two quantities collected at the monitoring wells. We use a Differential Evolution optimization algorithm to identify the optimal locations for the monitoring wells such that the measurements at these locations can predict, with the least error, the fields for peak concentration and peak time over the spatial domain of interest, regardless of which of the stochastic simulations from the groundwater model turns out to be the true state of nature.

This method was applied for designing a proof-of-concept optimal compliance monitoring network for an injection well field proposed for the injection of large volumes of coal seam gas produced water in the Surat Basin (Queensland, Australia). Optimal locations of 10 monitoring wells were identified using this approach. The method has the capability to simultaneously identify the optimal locations, and help inform the optimal times, for monitoring peak concentration.

#### Acknowledgments

We thank Mat Gilfedder and Tao Cui for reviewing and providing very useful comments for improving the presentation of this manuscript. We also thank the anonymous reviewers of this manuscript. The data used in this study can be accessed by sending an e-mail to Sreekanth.janardhanan@csiro.au.

### References

- Alzraiee, A. H., D. A. Bau, and L. A. Garcia (2013), Multiobjective design of aquifer monitoring networks for optimal spatial prediction and geostatistical parameter estimation, *Water Resour. Res.*, 49, 3670–3684, doi:10.1002/wrcr.20300.
- Ammar, K., A. Khalil, M. McKee, and J. Kaluarachchi (2008), Bayesian deduction for redundancy detection in groundwater quality monitoring networks, *Water Resour. Res.*, 44, W08412, doi:10.1029/2006WR005616.
- Asefa, T., M. W. Kemblowski, G. Urroz, M. McKee, and A. Khalil (2004), Support vectors-based groundwater head observation networks design, *Water Resour. Res.*, 40, W11509, doi:10.1029/2004WR003304.
- Asefa, T., M. Kemblowski, G. Urroz, and M. McKee (2005), Support vector machines (SVMs) for monitoring network design, *Ground Water*, 43, 413–422, doi:10.1111/j.1745-6584.2005.0050.x.
- Bierkens, M. F. P. (2006), Designing a monitoring network for detecting groundwater pollution with stochastic simulation and a cost model, *Stochastic Environ. Res. Risk Assess.*, 20(5), 335–351, doi:10.1007/s00477-005-0025-2.
- Bolster, D., M. Barahona, M. Dentz, D. Fernandez-Garcia, X. Sanchez-Vila, P. Trinchero, C. Valhondo, and D. M. Tartakovsky (2009), Probabilistic risk analysis of groundwater remediation strategies, *Water Resour. Res.*, 45, W06413, doi:10.1029/2008WR007551.

- Cameron, K., and P. Hunter (2000), *Optimization of LTM Networks Using GTS: Statistical Approaches to Spatial and Temporal Redundancy*, Air Force Cent. for Environ. Excellence, Brooks AFB, Tex.
- Chadalavada, S., and B. Datta (2008), Dynamic optimal monitoring network design for transient transport of pollutants in groundwater aquifers, *Water Resour. Manage.*, 22(6), 651–670, doi:10.1007/s11269-007-9184-x.
- Chadalavada, S., B. Datta, and R. Naidu (2011), Uncertainty based optimal monitoring network design for a chlorinated hydrocarbon contaminated site, *Environ. Monit. Assess.*, 173(1–4), 929–940, doi:10.1007/s10661-010-1435-2.
- Datta, B., and S. D. Dhiman (1996), Chance-constrained optimal monitoring network design for pollutants in ground water, *J. Water Resour. Plann. Manage.*, 122(3), 180–188, doi:10.1061/(ASCE)0733-9496(1996)122:3(180).
- Dhar, A., and B. Datta (2009), Logic-based design of groundwater monitoring network for redundancy reduction, *J. Water Resour. Plann. Manage.*, 122(3), 180–188, doi:10.1061/(ASCE)0733-9496(1996)122:3(180).
- Doherty, J. (2012), *Addendum to the PEST Manual*, Watermark Numer. Comput., Brisbane, Australia.
- Dokou, Z., and G. F. Pinder (2009), Optimal search strategy for the definition of a DNAPL source, *J. Hydrol.*, 376(3), 542–556, doi:10.1016/j.jhydrol.2009.07.062.
- Flemming, D. A., and T. G. Measham (2015), Local economic impacts of an unconventional energy boom: The coal seam gas industry in Australia, *Aust. J. Agric. Resour. Econ.*, 59(1), 78–94.
- Herrera, G. S., and G. F. Pinder (1998), Cost-effective groundwater quality sampling network design, in *Computational Methods in Water Resources XII*, vol. 1, pp. 51–58, doi:10.2495/CMWRI980071.
- Herrera, G. S., and G. F. Pinder (2005), Space-time optimization of groundwater quality sampling networks, *Water Resour. Res.*, 41, W12407, doi:10.1029/2004WR003626.
- Herrera, G., and R. Simuta-Champo (2013), Optimal design of groundwater-quality sampling networks with three-dimensional selection of sampling locations using an ensemble smoother, *J. Water Resour. Plann. Manage.*, 139(6), 682–692, doi:10.1061/(ASCE)WR.1943-5452.0000230.
- Herrera, G. S., J. Guaraccia, and G. F. Pinder (2000), A methodology for the design of space-time groundwater quality sampling networks, in *Proceedings of the XIII International Conference on Computational Methods in Water Resources*, vol. 1, pp. 579–585.
- Hudak, P. F., and H. A. Loaiciga (1992), A location modeling approach for groundwater monitoring network augmentation, *Water Resour. Res.*, 28(3), 643–649, doi:10.1029/91WR02851.
- Hudak, P. F., and H. A. Loaiciga (1993), An optimization method for monitoring network design in multilayered groundwater flow systems, *Water Resour. Res.*, 29(8), 2835–2845, doi:10.1029/93WR01042.
- James, B. R., and S. M. Gorelick (1994), When enough is enough: The worth of monitoring data in aquifer remediation design, *Water Resour. Res.*, 30(12), 3499–3513, doi:10.1029/94WR01972.
- Kollat, J. B., and P. Reed (2007), A framework for visually interactive decision-making and design using evolutionary multi-objective optimization (VIDEO), *Environ. Model. Software*, 22(12), 1691–1704, doi:10.1016/j.envsoft.2007.02.001.
- Kollat, J. B., P. M. Reed, and J. R. Kasprzyk (2008), A new epsilon-dominance hierarchical Bayesian optimization algorithm for large multiobjective monitoring network design problems, *Adv. Water Resour.*, 31(5), 828–845, doi:10.1016/j.advwatres.2008.01.017.
- Kollat, J. B., P. M. Reed, and R. M. Maxwell (2011), Many-objective groundwater monitoring network design using bias-aware ensemble Kalman filtering, evolutionary optimization, and visual analytics, *Water Resour. Res.*, 47, W02529, doi:10.1029/2010WR009194.
- Loaiciga, H. A., R. J. Charbeneau, L. G. Everett, G. E. Foggi, B. F. Hobbs, and S. Rouhani (1992), Review of ground-water quality monitoring network design, *J. Hydraul. Eng.*, 118(1), 11–37, doi:10.1061/(ASCE)0733-9429(1992)118:1(11).
- Mahar, P. S., and B. Datta (1997), Optimal monitoring network and ground-water-pollution source identification, *J. Water Resour. Plann. Manage.*, 123(4), 199–207, doi:10.1061/(ASCE)0733-9496(1997)123:4(199).
- Massmann, J., and R. A. Freeze (1987a), Groundwater contamination from waste management sites: The interaction between risk-based engineering design and regulatory policy: 1. Methodology, *Water Resour. Res.*, 23(2), 351–367, doi:10.1029/WR023i002p00351.
- Massmann, J., and R. A. Freeze (1987b), Groundwater contamination from waste management sites: The interaction between risk-based engineering design and regulatory policy: 2. Results, *Water Resour. Res.*, 23(2), 368–380, doi:10.1029/WR023i002p00368.
- McKinney, D. C., and D. P. Loucks (1992), Network design for predicting groundwater contamination, *Water Resour. Res.*, 28(1), 133–147, doi:10.1029/91WR02397.
- Meyer, P. D., and E. D. Brill Jr. (1988), A method for locating wells in a groundwater monitoring network under conditions of uncertainty, *Water Resour. Res.*, 24(8), 1277–1282, doi:10.1029/WR024i008p01277.
- Montas, H. J., R. H. Mohtar, A. E. Hassan, and F. A. Al Khal (2000), Heuristic space-time design of monitoring wells for contaminant plume characterization in stochastic flow fields, *J. Contam. Hydrol.*, 43(3), 271–301, doi:10.1016/S0169-7722(99)00108-4.
- Mullen, K. M., D. Ardia, D. Gil, D. Windover, and J. Cline (2011), DEoptim: An R package for global optimization by differential evolution, *J. Stat. Software*, 40(6), 1–26.
- National Water Quality Management Strategy (2014), *Guidelines for Groundwater Quality Protection in Australia 2013*, Aust. Gov., Canberra. [Available at <http://www.agriculture.gov.au/SiteCollectionDocuments/water/groundwater-quality-protection.pdf>.]
- Nghiem, L. D., T. Ren, N. Aziz, I. Porter, and G. Regmi (2011), Treatment of coal seam gas produced water for beneficial use in Australia: A review of best practices, *Desalination Water Treatment*, 32(1–3), 316–323.
- Nunes, L. M., M. C. Cunha, and L. Ribeiro (2004a), Optimal space-time coverage and exploration costs in groundwater monitoring networks, *Environ. Monit. Assess.*, 93(1–3), 103–124, doi:10.1023/B:EMAS.0000016795.91968.13.
- Nunes, L. M., M. C. Cunha, and Ribeiro, L. (2004b), Groundwater monitoring network optimization with redundancy reduction, *J. Water Resour. Plann. Manage.*, 130(1), 33–43, doi:10.1061/(ASCE)0733-9496(2004)130:1(33).
- Queensland Government (2016), *Surat Underground Water Impact Report – 2016, Summary*, Dep. of Nat. Resour. Manage., Off. of Groundwater Impact Assess., Brisbane, Australia. [Available at [https://www.dnrm.qld.gov.au/\\_data/assets/pdf\\_file/0008/345680/uwir-2016-summary.pdf](https://www.dnrm.qld.gov.au/_data/assets/pdf_file/0008/345680/uwir-2016-summary.pdf).]
- R Core Team (2015), *R: A Language and Environment for Statistical Computing*, R Found. for Stat. Comput., Vienna. [Available at <http://www.R-project.org/>.]
- Reed, P., B. Minsker, and A. J. Valocchi (2000), Cost-effective long-term groundwater monitoring design using a genetic algorithm and global mass interpolation, *Water Resour. Res.*, 36(12), 3731–3741, doi:10.1029/2000WR900232.
- Reed, P., B. S. Minsker, and D. E. Goldberg (2003), Simplifying multiobjective optimization: An automated design methodology for the non-dominated sorted genetic algorithm-II, *Water Resour. Res.*, 39(7), 1196, doi:10.1029/2002WR001483.
- Reed, P. M., and B. S. Minsker, (2004), Striking the balance: Long-term groundwater monitoring design for conflicting objectives, *J. Water Resour. Plann. Manage.*, 130(2), 140–149, doi:10.1061/(ASCE)0733-9496(2004)130:2(140).
- Ruiz-Cárdenas, R., M. A. R. Ferreira, and A. M. Schmidt (2010), Stochastic search algorithms for optimal design of monitoring networks, *Environmetrics*, 21(1), 102–112, doi:10.1002/env.989.

- Sreekanth, J., and B. Datta (2011), Optimal combined operation of production and barrier wells for the control of saltwater intrusion in coastal groundwater well fields, *Desalination Water Treatment*, 32(1–3), 72–78.
- Sreekanth, J., and B. Datta (2013), Design of an optimal compliance monitoring network and feedback information for adaptive management of saltwater intrusion in coastal aquifers, *J. Water Resour. Plann. Manage.*, 140(10), 04014026, doi:10.1061/(ASCE)WR.1943-5452.0000406.
- Sreekanth, J., B. Datta, and P. K. Mohapatra (2012), Optimal short-term reservoir operation with integrated long-term goals, *Water Resour. Manage.*, 26(10), 2833–2850.
- Storck, P., J. W. Eheart, and A. J. Valocchi (1997), A method for the optimal location of monitoring wells for detection of groundwater contamination in three-dimensional heterogenous aquifers, *Water Resour. Res.*, 33(9), 2081–2088, doi:10.1029/97WR01704.
- Storn, R., and K. Price (1997), Differential evolution—A simple and efficient heuristic for global optimization over continuous spaces, *J. Global Optim.*, 11(4), 341–359, doi:10.1023/A:1008202821328.
- Tonkin, M., and J. Doherty (2009), Calibration-constrained Monte Carlo analysis of highly parameterized models using subspace techniques, *Water Resour. Res.*, 45, W00B10, doi:10.1029/2007WR006678.
- Wu, W. M., et al. (2006), Pilot-scale in situ bioremediation of uranium in a highly contaminated aquifer: 1. Conditioning of a treatment zone, *Environ. Sci. Technol.*, 40(12), 3978–3985, doi:10.1021/es051954y.
- Wu, Y. (2004), Optimal design of a groundwater monitoring network in Daqing, China, *Environ. Geol.*, 45(4), 527–535, doi:10.1007/s00254-003-0907-x.
- Zhang, Y., G. F. Pinder, and G. S. Herrera (2005), Least cost design of groundwater quality monitoring networks, *Water Resour. Res.*, 41, W08412, doi:10.1029/2005WR003936.